LAWRENCE
LIVERMORE
NATIONAL
LABORATORY

UCRL-CONF-216907

Corrosion Behavior of Alloy 22 in Chloride Solutions Containing Organic Acids

R. M. Carranza, C. M. Giordano, M. A.Rodríguez, R. B. Rebak

November 8, 2005

CORROSION/2006 Conference and Exposition
San Diego, CA, United States
March 12, 2006 through March 16, 2006

Disclaimer

CORROSION BEHAVIOR OF ALLOY 22 IN CHLORIDE SOLUTIONS CONTAINING ORGANIC ACIDS

Ricardo M. Carranza, C. Mabel Giordano, Martín A. Rodríguez
Comisión Nacional de Energía Atómica
Av. Gral. Paz 1499
San Martín, Buenos Aires, 1650, Argentina

Raúl B. Rebak
Lawrence Livermore National Laboratory
PO Box 808 L-631, 7000 East Ave.
Livermore, CA, 94550

ABSTRACT

Alloy 22 (N06022) is a nickel based alloy containing alloying elements such as chromium, molybdenum and tungsten. It is highly corrosion resistant both under reducing and under oxidizing conditions. Electrochemical studies such as electrochemical impedance spectosopy (EIS) were performed to determine the corrosion behavior of Alloy 22 in 1M NaCl solutions at various pH values from acidic to neutral at 90ºC . Tests were also carried out in NaCl solutions containing oxalic acid or acetic acid. It is shown that the corrosion rate of Alloy 22 was higher in a solution containing oxalic acid than in a solution of the same pH acidified with HCl. Acetic acid was not corrosive to Alloy 22. The corrosivity of oxalic acid was attributed to its capacity to form stable complex species with metallic cations from Alloy 22.

Keywords: Alloy 22, N06022, organic acids, oxalic, acetic, pH, corrosion rate

INTRODUCTION

Alloy 22 (N06022) contains by weight approximately 22% chromium (Cr), 13% molybdenum (Mo), 3% tungsten (W) and approximately 3% iron (Fe). Alloy 22 was commercially designed to resist the most aggressive industrial applications, offering a lo

general corrosion rate both under oxidizing and reducing conditions.[1] Under oxidizing and acidic conditions Cr exerts its beneficial effect in the alloy. Under reducing conditions the most beneficial alloying elements are Mo and W, which offer a low current for hydrogen discharge.[2,3] Moreover, due to its balanced content in Cr, Mo and W, Alloy 22 is used extensively in hot chloride containing environments where austenitic stainless steels may fail by pitting corrosion and stress corrosion cracking (SCC).[1,2,3]

Alloy 22 is the material selected for the fabrication of the outer shell of the nuclear waste containers for the Yucca Mountain site.[4,5] Several papers have been published recently describing the general and localized corrosion behavior of Alloy 22 regarding its application for the nuclear waste containers.[6,7,8] It is also known that the addition of nitrate and other oxyanions to a chloride-containing environment, decreases the susceptibility of Alloy 22 to localized attack.[9,10] It has been recently reported that fluoride ions may also act as an inhibitor to crevice corrosion of in Alloy 22.[11] Little is known on the corrosion behavior of Alloy 22 in organic acids.[12] It was shown that the corrosion rate of Alloy 22 increases as the concentration of oxalic acid increased from 0.01 M to 1 M. For a concentration of oxalic acid of 0.1 M, the corrosion rate increased as the temperature increased from 30°C to 90°C. Oxalic acid did not promote localized corrosion such as crevice corrosion in Alloy 22.[12]

The objective of the current study was to use electrochemical methods and parameters to systematically assess the corrosion behavior of Alloy 22 (N06022) in oxalic and acetic acids solutions as compared to the behavior in sodium chloride solutions of the same pH.

Oxalic acid or ethanedioic (HOOCCOOH or H2O4C2) is an organic acid widely used in the pharmaceutical industry as an intermediate or as a component. Oxalic acid is also used as bleaching agent in the textile industry, as a precipitation agent in the production of rare earths, as a rust remover, in water treatment, etc. Oxalic acid is one of the most aggressive alkane acids. Oxalic acid is slightly oxidizing with dissociation constants pKa1 = 1.25 and pKa2 = 3.81 (Table 1).[13] Table 1 also shows the complexing properties of oxalic acid when reacting with metal cations (Equation 1):[14]

$$M + n\,L \Leftrightarrow ML_n \qquad (1)$$

Where M are metal ions (e.g. Cr, Ni) L is the ligand (e.g. oxalic acid) and ML_n is the metal complex.

Acetic acid or ethanoic (CH3COOH or H4O2C2) is fabricated industrially by reaction of carbon monoxide and methanol. The primary use of acetic acid in the industry is to make acetate esters including cellulose acetate (used in films and clothing fabrics) and polyvynil acetate (latex paints and glue). Another important use of acetic acid is in the production of aspirin (acetylsalicylic acid). Acetic acid is classified as a weak acid, because it does not completely dissociate into its component ions when dissolved in aqueous solutions. At a concentration of 0.1 M, only about 1% of the molecules are ionized. The dissociation constant for acetic acid is pKa1 = 4.76; that is, for the same acid concentration in water, acetic acid will give a higher value of pH than oxalic acid (Table 1). Table 1 also shows the complexing properties of acetic acid with metal cations. Complexes of oxalic acid seem orders of magnitude more stable than the complexes of acetic acid with the same cations.

Fungi and bacteria can decompose organic matter to produce organic acids.[15,16,17,18,19,20] Some of these organic acids include: oxalic, acetic, propionic, formic, citric,

butyric, etc. In general acetic acid accounted for 60-80% of all the acids produced when bacteria decomposes starch.[18,20] The concentration of acetic acid as a product could be 15.3 g/L (0.25 M). The fungus Aspergillus Niger can produce oxalic acid.[15,16] Laboratory studies have shown that A. niger and Penicillium can produce small amounts of oxalic acid, in the order of 0.00018 M (or 18 ppm). It must also be considered that this acid production must represent a high concentration condition, since the microorganisms were provided with nutrients (such as glucose). On the other hand, it is difficult to assess the concentration of the organic acid in a local spot, for example below biofilms. That is, it is not simple to predict with certainty what could be the concentration of oxalic acid in contact with a buried metallic container due to microbial activity. It is expected to be low (below 0.0001 M), first because the supply of organic matter is limited and second because oxalic acid reacts with some earth cations to form insoluble oxalate salts. For example, the solubility of calcium oxalate at 13°C is 0.00067 g/100 cc of water and at 95°C is 0.0014 g/100 cc of water. These two amounts translate into 6.7 ppm (or 0.000074 M) and 14 ppm (or 0.00015 M).

EXPERIMENTAL PROCEDURE

Specimens of Alloy 22 were prepared from wrought mill annealed plate stock (MA specimens). The chemical composition of the alloy in weight percent was 59.20% Ni, 20.62% Cr, 13.91% Mo, 2.68% W, 2.80% Fe, 0.01% Co, 0.14% Mn, 0.002% C, and 0.0001% S. Parallelepiped specimens measuring 12 mm x 12 mm x 15 mm were mounted with a polytetrafluoroethylene (PTFE) compression gasket (ASTM G 5)[21]. A torque was applied to the gasket to ensure a leak-proof assembly. The occluded area from the PTFE gasket was 0.75 cm^2 and the exposed area of the specimen was 10.5 cm^2. The specimens had a finished grinding of abrasive paper number 600 and were degreased in acetone and washed in distilled water 1 hour prior to testing.

Electrochemical measurements were conducted in a three-electrode, borosilicate glass cell. A water-cooled condenser combined with a water trap was used to avoid evaporation and the ingress of air. Solution temperature was controlled by immersing the cell in a thermostatized water bath. The cell was equipped with both an air cooled Luggin and a saturated calomel reference electrode (SCE) which has a potential of 0.242 V more positive than the standard hydrogen electrode (SHE). A large area platinum wire was used as counter electrode. The electrochemical tests were carried out in 1M NaCl solutions, at different pH values between 1 and 6, with and without the addition of acetic or oxalic acids. Small amounts of HCl were added in order to adjust solution pH of pure NaCl solutions. The test temperature was 90.0 $\pm$ 0.1ºC. Solutions were prepared with analytical grade chemicals and 18.2 MΩ resistivity water. Solution pH was determined at room temperature using a calibrated (GLP-conform protocol of calibration) pH meter together with a pH electrode with temperature sensor (measuring pH range = 0 to 14, operating temperature range = -5ºC to 80ºC, gel reference electrolyte, internal buffer pH = 7.0 $\pm$ 0.25, fiber diaphragm, cylindrical glass membrane resistance = 300 MΩ at 25ºC) calibrated using two buffer solutions of pH 7.00 and 1.01. Solutions for the cyclic potentiodynamic polarization curves were deaerated with nitrogen. Solutions for EIS measurements were naturally aerated, that is, air was not bubbled through the solution.

The cyclic potentiodynamic polarization technique (CPP) (ASTM G 61) was used to determine the electrochemical characteristics of Alloy 22 in these media. The specimen was attached to the connecting rod via a PTFE gasket which provided an artificial metal/non metal

crevice. Before immersing the testing specimens, the solutions were purged with nitrogen for an hour and this was maintained throughout the tests. No effect on the measured currents during polarization was observed due to solution stirring during bubbling. The potential scan was started 150 mV below the initial corrosion potential. The scan rate used was 0.167 mV/s, and the scan direction was reversed when the current reached 1-10 mA/cm^2. At the conclusion of the test, the specimens were examined microscopically for signs of corrosion.

Electrochemical Impedance Spectroscopy (EIS) measurements were carried out at the corrosion potential in natural aerated solutions (without nitrogen bubbling). A 5 mV amplitude sinusoidal potential signal was superimposed to the corrosion potential. The frequency scan was started at 10 kHz and ended at 1 mHz. In order to model the impedance results with electrical analogs, a simplified R//CPE series equivalent circuit (Figure 1) was fitted to the experimental results using the complex nonlinear least squares (CNLS) method. From the obtained fitting parameters the low frequency or polarization resistance (R_P) was used to calculate the corrosion rate using equation (2) assuming a linear relationship between R_P^{-1} and the corrosion rate (CR) as it is usually done[22,23]:

$$CR(mm/yr) = \frac{K \quad B \quad EW}{\rho} \frac{1}{R_P} \qquad (2)$$

where EW is the equivalent weight (23.28, assuming congruent dissolution of the major alloying elements as Ni^{2+}, Cr^{3+}, Mo^{3+}, Fe^{3+}, and W^{4+}), K is the faradic conversion factor (3,270 mm g A^{-1} cm^{-1} yr^{-1}), ρ is the density (8.69 g/cm^3)(ASTM G102), Rp is the low frequency resistance in $ohm.cm^2$ and B is the Stern and Geary constant[24] expressed in Volts. The latter can be calculated using Tafel slopes attributed to the anodic and the cathodic processes occurring at E_{corr}. Macdonald *et al* found a constant passivation current density independent of the potential for Alloy 22 in NaCl brine at 80ºC, this indicate that the Stern and Geary constant would be dominated by the cathodic Tafel slope β_c ($B = \beta_c / 2.303$), but in a previous paper[25] they measured the anodic (different from ∞) and cathodic Tafel slopes using potentiodynamic polarization curves, obtaining B values between 24 and 46 mV for solution pH values varying from 1.0 to 8.1. In the present work the B constant used in calculating the corrosion rate was assumed to be 26 mV (the all purpose middle value, expected for both theoretically calculated and experimentally observed values, as proposed by Mansfeld[26]) independently of the solution composition and pH, and it is not intended to represent the real value of the B constant but a mean value used to compare the influence of environmental variables (such as pH) on the corrosion performance of Alloy 22.

RESULTS AND DISCUSSION

Cyclic Potentiodynamic Polarization (CPP)

Figure 2 shows typical CPP curves obtained for Alloy 22 in deaerated 1M NaCl solutions at different pH values from pH 1 to pH 6. An anodic peak could be observed at the potentials near to the corrosion potential. The higher the acidity of the solution the more pronounced the anodic peak. Passivity currents increased slightly with decreasing pH between pH 6 and 1. Transpassivity potential values decreased with increasing pH, being approximately 0.80 V_{sce} for pH 1 and 0.25 V_{sce} for pH 6. Reverse scans of the polarization curves did not generally show significant hysteresis. Examination of the tested specimens

showed that they were generally free from crevice corrosion under the PTFE compression gasket.

Figure 3 shows the CPP curves obtained for Alloy 22 in deaerated 1M NaCl with the addition of different concentrations of acetic acid. All the curves showed similar behavior. Only small differences could be detected in their corrosion potentials, passive current densities and transpassive potentials. While the pH for all the solutions was in the range of approximately 3 to 4, the acetic acid concentration changed from 0.1 M down to a nil concentration (pH 3 due to the addition of small amounts of HCl) from one solution to another. This means that the acetic acid concentration has no effect on the electrochemical parameters other than that produced by the change in pH.

Figure 4 show the CPP curves obtained for Alloy 22 in deaerated 1M NaCl with the addition of different concentrations of oxalic acid. It can be observed that passive currents increased significantly when the pH was decreased from approximately 4 to 1. The variation in current was significantly higher than that produced for the same pHs in the absence of oxalic acid, indicating that the oxalic acid has an aggressive behavior in the passive region apart from that produced due to the decrease in pH. Figure 4 shows a comparison of the CPP curves for solutions with and without the addition of oxalic acid at pH 2.0. It can be clearly seen that the main effect of the addition of oxalic acid was to increase the passive current density, while the transpassive behavior was not significantly modified.

Figure 6 shows the variation of the transpassivity potentials E_{20} (the potential at which anodic current equals 20 $\mu A/cm^2$ in the forward potential scan[27;28]). It can be seen that E_{20} was a function of solution pH and was independent of the solution composition. A large scatter of E_{20} values was observed only for 1M NaCl at pH 4. Due to the low buffer capacity of this solution its pH changed throughout the test. The linear least squares fit applied to the E_{20} values as a function of the solution pH, excluding those for 1M NaCl at pH 4, gave the following relationship:

$$E_{20} (V_{SCE}) = 0.869 - 0.071\ pH \quad \text{with} \quad R^2 = 0.937 \qquad (3)$$

The slope of the E_{20} *vs* pH curve rendered 71mV per pH unit. All nickel oxides (including $Ni(OH)_2$) would present a similar behavior (72 mV per pH unit at 90ºC) according to thermodynamic data.[29] Chromium dissolution to chromates or dichromates would present higher pH dependences.

Corrosion Rate (CR)

Figures 7, 8 and 9 show, as examples, EIS diagrams obtained for Alloy 22 in aerated solutions 1M NaCl at pH 2, 1M NaCl + 0.01M oxalic acid, and 1M NaCl + 0.1M oxalic acid respectively, after 1h and 24h of immersion at 90ºC in aerated solutions. In the same diagrams the result of the CNLS fittings of the R//CPE equivalent circuit (Figure 1) is showed as solid lines. It can be seen that fairly good fittings were obtained despite the simplicity of the equivalent circuit used. Deviations between model and experimental results were more significant at low frequencies. These deviations may be attributed to both current drifts (each diagram took more than 2h to be completed and the low frequency points made used of most of this time) and oversimplification of the equivalent circuit used to model the experimental diagrams.

For all the systems tested in this work the Bode diagrams obtained after 1h of immersion showed two well separated time constants (observed as two maxima in the phase curve). The high frequency time constants, at the more cathodic potentials (not in the full passive range) were interpreted previously[30] as associated to the cathodic reactions and to the oxidation of Ni at potentials closer to the reversible potential where the oxide layer is assumed to be thinner. After 24-h of immersion the diagrams could generally be fitted considering only one R//CPE time constant (except for solutions of the lowest pH values, i.e. that containing 0.1M oxalic acid, Figure 9). In all the cases the low frequency resistance (R_P) was considered to be related to the corrosion rate as was is shown in Equation (2). In the Nyquist diagrams of Figures 7 to 9 only the low frequency time constants are evident and the differences on R_P between 1h and 24h of immersion are prominent.

Figure 10 shows the corrosion rates calculated for all the solutions tested in this work as a function of the time of immersion at the open circuit potential up to 24h. It can be seen that, as a general rule, corrosion rates decreased significantly with time except for the solutions containing oxalic acid and for 1M NaCl solution pH 1. In these cases the decrease in corrosion rate was smaller and for 0.1M oxalic acid it even increased after 24h of immersion. Corrosion rate reduction with time of immersion in NaCl solutions at pH 6 is attributed to both film thickening and film improvement due to annihilation of defects.

Figure 11 shows the evolution with time of the corrosion potential in aerated solution: 1M NaCl solutions and in 1M NaCl + oxalic acid. It can be seen that the corrosion potential increased with time for the highest pH values, moving from potentials in the active anodic peak zone to potentials in the full passive range according to the values obtained from the CPP curves (Figures 2 and 4). The corrosion potential of all the solutions containing acetic acid (not shown) behaved this way. On the other hand, for the lowest pH value the corrosion potential increased slightly for pure NaCl solutions (pH 1) and remained almost constant for 1M NaCl + 0.1M oxalic acid (pH 1.3) indicating, that the system remained in the active zone. Consequently, for the 0.1M oxalic acid solution, the Bode diagrams after 24h of immersion presented two time constants (Figure 9).

Figure 12 shows the corrosion rate measured by means of the EIS technique after 24 hours of immersion in natural aerated solutions. It can be seen that corrosion rates of oxalic acid containing solutions were higher than those corresponding to NaCl solutions at the same pH. This fact implies that oxalic acid had an additional effect, aside from the pH effect, on the corrosion rate of Alloy 22. This effect remained active independently of the potential zone in which E_{corr} was located (active zone for 0.1M solution and passive zone for lower concentrations). Acetic acid containing solutions produced no increase in corrosion rates compared with NaCl solutions of the same pH (Figure 12). The difference between oxalic and acetic acids is their complexing strength as was shown in Table 1. Oxalic acid produced higher metallic dissolution due to his strong metallic complexing character and its influence could be clearly detected for concentrations higher than 0.001M in 1M NaCl solutions. On the contrary, this strong metallic complexing character seemed not to enhance transpassive dissolution, as was shown in Figure 4.

Further research is needed to elucidate the effect of organic acids on the transpassive dissolution and also on crevice corrosion susceptibility of Alloy 22 when mixed with chloride ions.

CONCLUSIONS

1. Corrosion rates of Alloy 22 after 24h of immersion in 1M NaCl solutions with the addition of oxalic acid in concentrations ranging from 0.1M to 0.001M were higher than those obtained for pure 1M NaCl solutions at the same pH, while the addition of the same concentrations of acetic acid produced no corrosion rate increase. This fact was attributed to the higher metallic complexing strength of oxalic compared to acetic.

2. Higher passive current densities were found during cyclic potendtiodynamic polarization of Alloy 22 in solutions containing oxalic acid compared to 1M NaCl solutions at the same pH values.

3. The transpassivity potential (E_{20}) was dependent on solution pH: E_{20} (V_{SCE}) = 0.869 – 0.071 pH, but showed no variation with the organic acid concentration or nature if compared to 1M NaCl solutions at the same pH values.

AKNOWLEDGEMENTS

This work was performed under the auspices of the U. S. Department of Energy (DOE) by the University of California Lawrence Livermore National Laboratory under contract N° W-7405-Eng-48, and supported by the Yucca Mountain Project, which is part of the Office of Civilian Radioactive Waste Management (OCRWM).

R. M. Carranza acknowledges financial support from the Agencia Nacional de Promoción Científica y Tecnológica of the Ministerio de Educación, Ciencia y Tecnología from Argentina.

DISCLAIMER

REFERENCES

1 R. B. Rebak and P. Crook, “Influence of the Environment on the General Corrosion Rate of Alloy 22 (N06022)”, Proceedings from Pressure Vessels and Piping Conference, 25-29 July 2004, San Diego, CA, PVP-Vol. 483, p. 131 (ASME, 2004: New York, NY).

2 R. B. Rebak and P. Crook, Advanced Materials and Processes, 37, February 2000.

3 R. B. Rebak in Corrosion and Environmental Degradation, Volume II, p. 69 (Wiley-VCH,2000: Weinheim, Germany).

4 G. M. Gordon, Corrosion, 58, 811 (2002).

5 Yucca Mountain Science and Engineering Report, U. S. Department of Energy, Office of Civilian Radioactive Waste Management, DOE/RW-0539, Las Vegas, NV, May 2001.

6 R. B. Rebak, Paper 05610, Corrosion/2005 (NACE Internacional, 2005: Houston, TX).

7 F. Hua, G. M. Gordon, K. G. Mon and R. B. Rebak, Paper 06619, Corrosion/2006 (NACE Internacional, 2005: Houston, TX).

8 G. S. Frankel, “Corrosion Reliability Prediction: Long Term Nuclear Waste Storage in Yucca Mountain, Proceedings from the 16th Internacional Corrosion Congress, 19-24 September 2005, Beijing, China.

9 D. S. Dunn, L. Yang, C. Wu and G. A. Cragnolino, Mat. Res. Soc. Symp. Proc. Vol 824 (MRS, 2004: Warrendale, PA)

10 D. S. Dunn, Y.-M. Pan, K. Chiang, L. Yang, G. A. Cragnolino and X. He, “Localized Corrosion Resistance and Mechanical Properties of Alloy 22 Waste Package Outer Containers” JOM, January 2005 (TMS, 2005: Warrendale, PA)

11 R. M Carranza, M. A. Rodríguez and R. B. Rebak, Paper 06622, Corrosion/2006 (NACE Internacional, 2005: Houston, TX).

12 S. D. Day, M. T. Whalen, K. J. King, G. A. Hust, L. L. Wong, J. C. Estill and R. B. Rebak, Corrosion, 60, 804 (2004).

13 CRC Handbook of Chemistry and Physics, David R. Lide, Ed., 85th Edition, CRC Press LLC, NY, 2004.

14 Critical Stability Constants, R. M. Smith and A. E. Martell, eds., Plenum Press, NY, 1976.

15 R. J. Palmer Jr., J. Siebert and P. Hirsch, Microbial Ecology, 21, 253 (1991).

16 P. Hirsch, F. E. W. Eckhardt and R. J. Palmer Jr., Can. J. Botany, 73, 1384 (1995).

17 J. M. Schrickx, M. J. H. Raedts, A. H. Stouthamer and H. W. van Verseveld, Analytical Biochem., 231, 175 (1995).

18 C. Sans, J. Mata-Alvarez, F. Cecchi, P. Pavan and A. Bassetti, Bioresource Technol., 51, 89 (1995).

19 D. A. Rockert, C. E. Glatz and B. A. Glatz, Enzyme and Microbial Technol., 22, 409 (1998).

20 J. Yu, J. Biotechnology, 86, 105 (2001).

21 Annual Book of ASTM Standards, Volume 03.02, American Society for testing and Materials, West Conshohocken, PA (2001).

22 D. D. Macdonald, A. Sun, N. Priyantha, P. Jayaweera, *J. Electroanal. Chem*., 2004, **572**, 421-431.

23 D.D. Macdonald, M.C.H. McKubre, in Impedance Spectroscopy, Theory, Experiment, and Applications, E. Barsoukov, J.R. Macdonald eds., JW & Sons, NJ, 2005, 343.

24 M. Stern, A. L. Geary, *J. Electrochem. Soc.*, 1957, **104**, 56.

25 N. Priyantha, P. Jayaweera, D. D. Macdonald, A. Sun, *J. Electroanal. Chem*., 2004, **572**, 409-419.

26 F. Mansfeld, in Adv. In Corrosion Science and Technology Vol. VI, M. G. Fontana and R. W. Staehle, eds., Plenum Press, New York, 1976, 163-262.

27 Kenneth J. Evans, Ahmet Yilmaz, S. Daniel Day, Lana L. Wong, John C. Estill, and Raúl B. Rebak, Journal of Metals, January 2005, pp. 56-61.

28 Keneth J. Evans, Lana N. Wong, and Raúl B. Rebak, PVP2004-2794, Vol. 483, Transportation, Storage, and Disposal of Radioactive Materials, July 25-29, San Diego, California, USA, (2004).

29 Atlas of Electrochemical Equilibria in Aqueous Solutions, Marcel Pourbaix, NACE, Houston, Texas, USA, c.1974, p.333.

30 R. M. Carranza, M. A. Rodríguez, R. B. Rebak, Passivity of Alloy 22 in Chloride and Fluoride Containing Solutions, in 16th International Corrosion Congress, September 19-24, 2005, Beijing, China, paper 6-2, 2005.

TABLE 1

DISSOCIATION AND METAL COMPLEX EQUILIBRIUM (FORMATION) CONSTANTS FOR ACETIC AND OXALIC ACIDS AT 25ºC. M: METAL CATION. L: ORGANIC LIGAND. ML_n: METAL COMPLEX. FIGURES BETWEEN BRACKETS INDICATE THE IONIC FORCE OF THE SOLUTION.

		Acetic Acid	Oxalic Acid
DISSOCIATION CONSTANTS			
$\log K_1$		- 4.756	- 1.25
$\log K_2$		---	- 3.81
METAL COMPLEX EQUILIBRIUM CONSTANTS			
Cr^{2+}	$\log(ML/M.L)$	1.25 (0.3) 1.80 (0)	3.85 (0.1)
	$\log(ML_2/M.L^2)$	2.15 (0.3) 2.92 (0)	6.81 (0.1)
Cr^{3+}	$\log(ML/M.L)$	4.63 (0.3)	NA
	$\log(ML_2/M.L^2)$	7.08 (0.3)	NA
	$\log(ML_3/M.L^3)$	9.6 (0.3)	NA
Ni^{2+}	$\log(ML/M.L)$	0.74 (0.5) 0.83-0.1 (1.0) 1.43 (0)	5.16 (0)

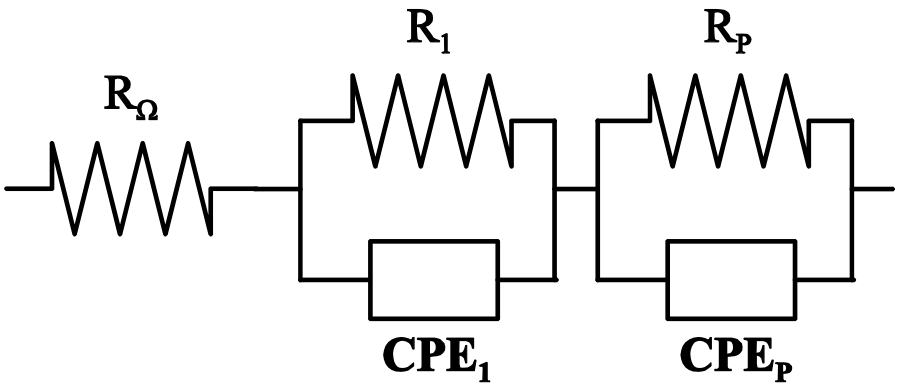

FIGURE 1: Equivalent circuit fitted to the experimental EIS diagrams using the CLNS method. R: Resistance. CPE: Constant Phase Element. Subscript 1: High frequency parameter. Subscript P: low frequency parameter. R_Ω: solution resistance. R_P: polarization or low frequency resistance.

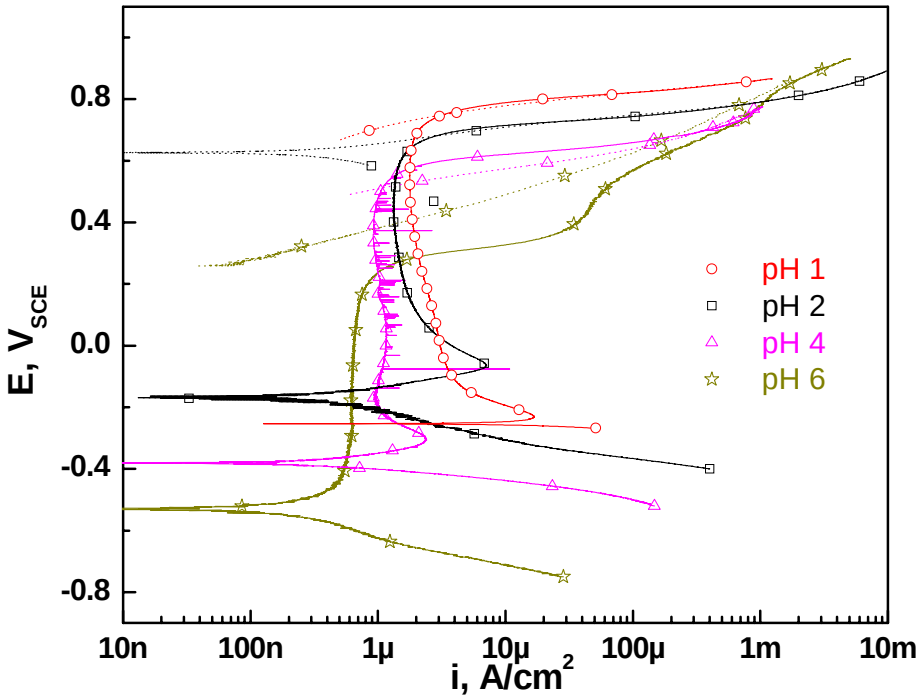

FIGURE 2: CPP curves for Alloy 22 in deaerated 1M NaCl solutions at 90ºC. Solid lines: direct scan. Dotted lines: reverse scan.

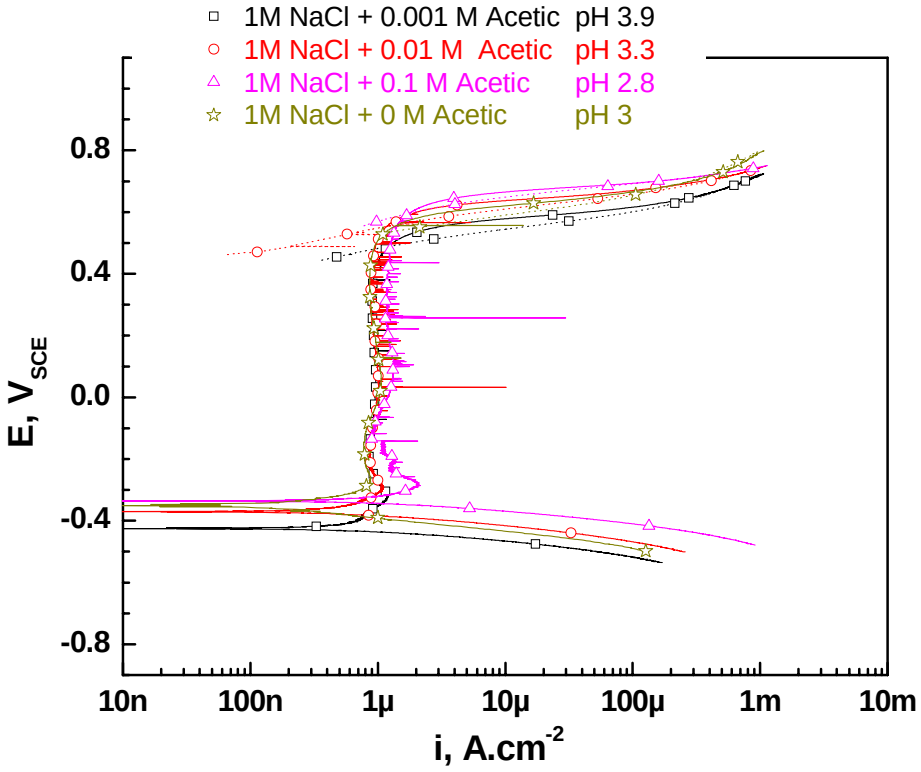

FIGURE 3: CPP curves for Alloy 22 in deaerated 1M NaCl solutions with the addition of acetic acid at 90ºC. Solid lines: direct scan. Dotted lines: reverse scan.

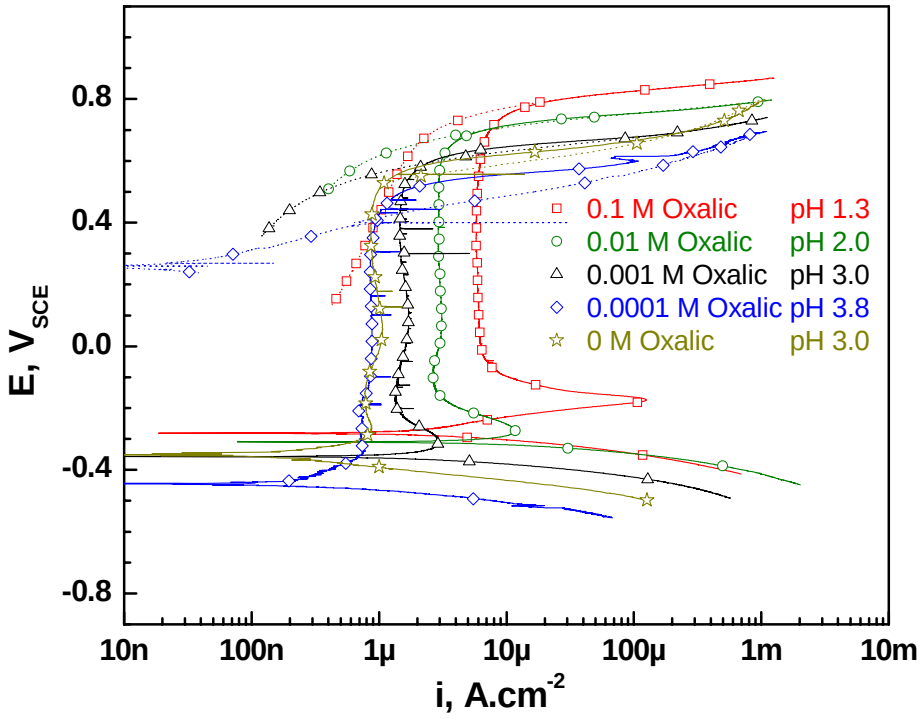

FIGURE 4: CPP curves for Alloy 22 in deaerated 1M NaCl solutions with the addition of oxalic acid at 90ºC. Solid lines: direct scan. Dotted lines: reverse scan.

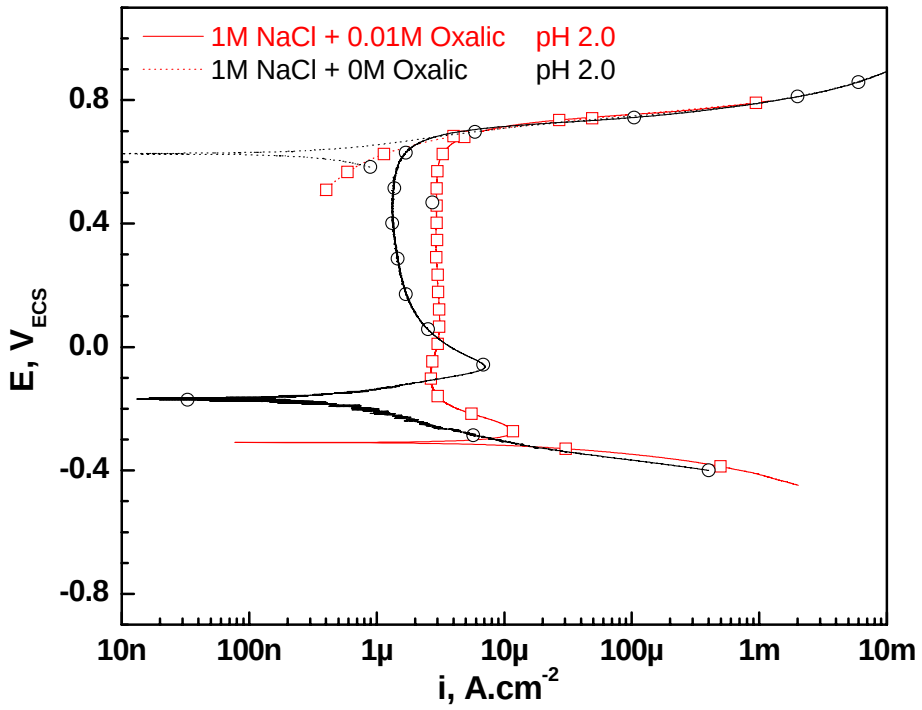

FIGURE 5: CPP curves for Alloy 22 in deaerated 1M NaCl and 1M NaCl + 0.01M oxalic acid at 90ºC . Solid lines: direct scan. Dotted lines: reverse scan.

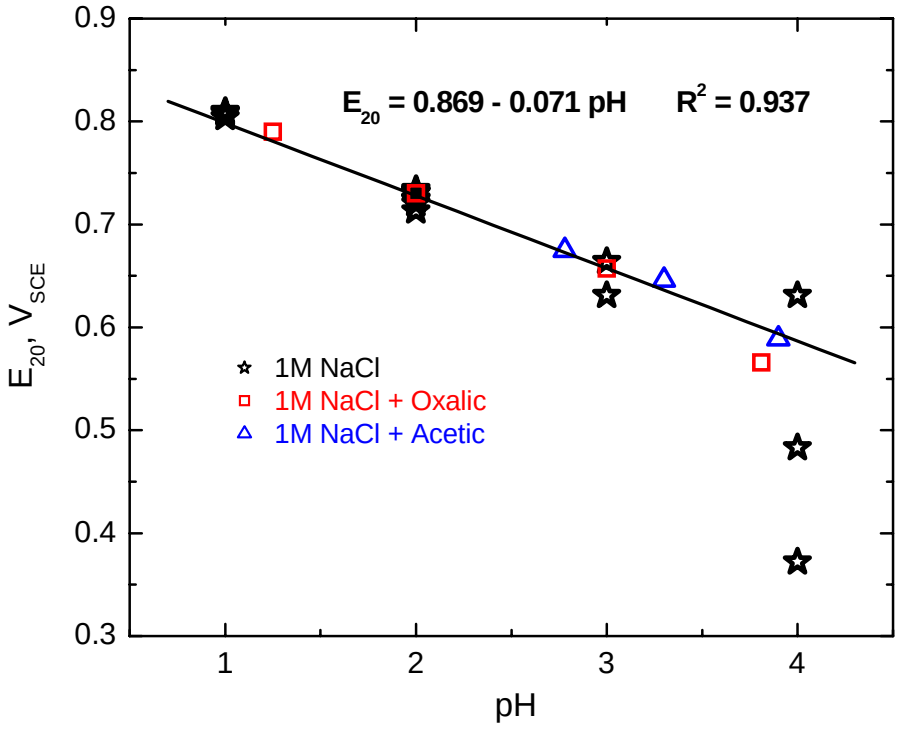

FIGURE 6: Variation of transpassivity potencial E_{20} with solution pH for Alloy 22 in deaerated 1M NaCl solutions with the addition of acetic or oxalic acid at 90ºC. Solid line: linear fit excluding 1M NaCl points at pH 4.

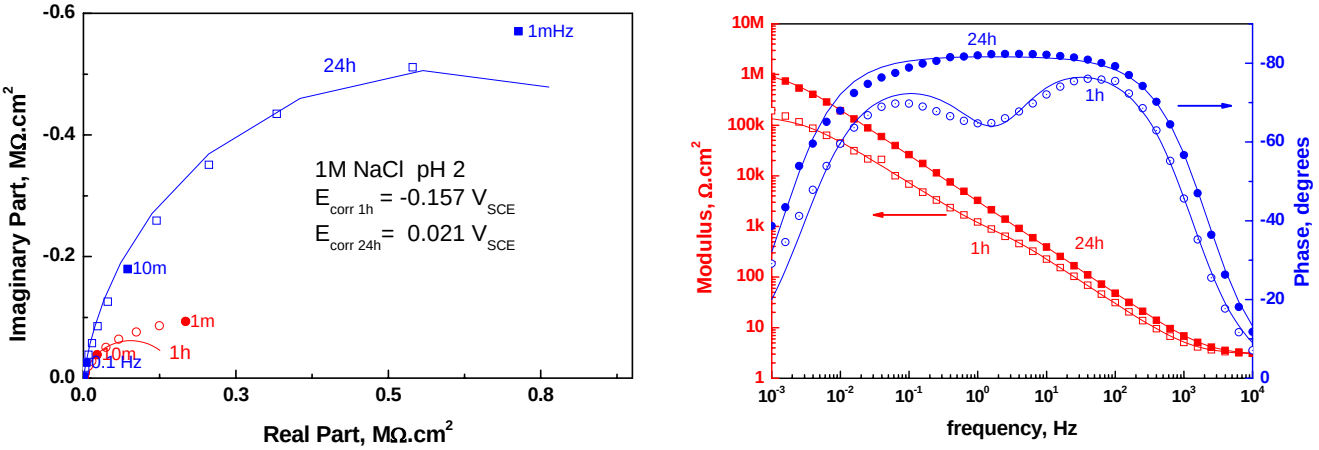

FIGURE 7: EIS diagrams obtained for Alloy 22 in aerated 1M NaCl pH 2 at the open circuit potential after 1h (E_{corr1h}= -0.157 V_{SCE}) and 24h ($E_{corr24h}$= -0.021 V_{SCE}) of immersion at 90ºC. Left: Nyquist diagrams. Right: Bode diagrams. Symbols: experimental results. .Lines: theoretical CNLS fitting using equivalent circuit of Figure 1.

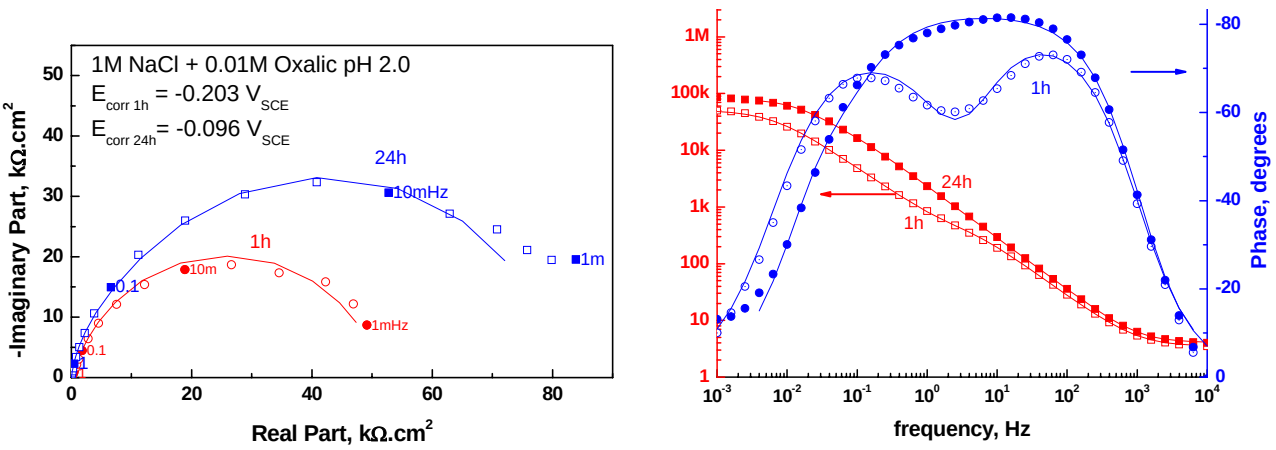

FIGURE 8: EIS diagrams obtained for Alloy 22 in aerated 1M NaCl + 0.01M oxalic acid pH 2.0 at the open circuit potential after 1h (E_{corr1h}= -0.203 V_{SCE}) and 24h ($E_{corr24h}$= -0.096 V_{SCE}) of immersion at 90ºC. Left: Nyquist diagrams. Right: Bode diagrams. Symbols: experimental results. .Lines: theoretical CNLS fitting using equivalent circuit of Figure 1.

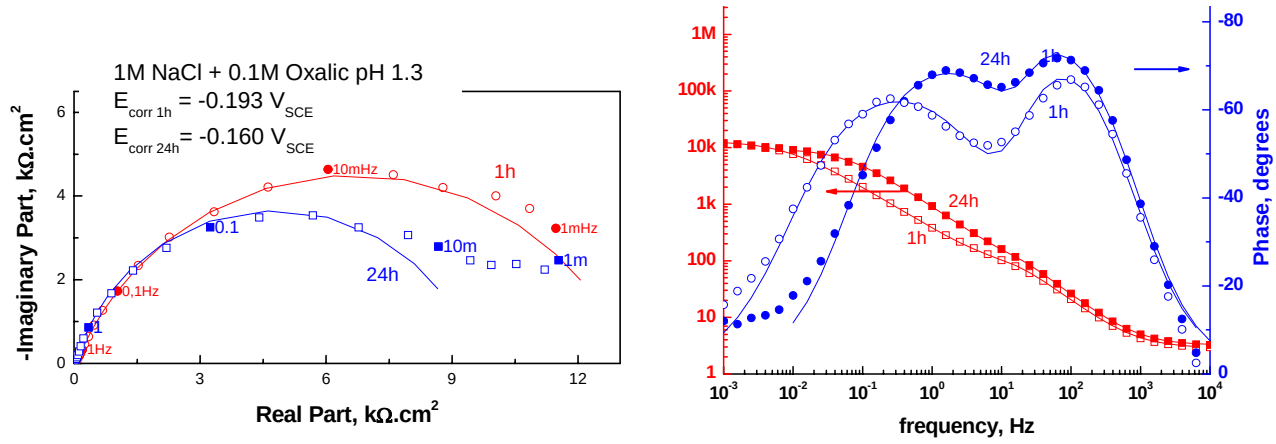

FIGURE 9: EIS diagrams obtained for Alloy 22 in aerated 1M NaCl + 0.1M oxalic acid pH 1.3 at the open circuit potential after 1h (E_{corr1h}= -0.193 V_{SCE}) and 24h ($E_{corr24h}$= -0.160 V_{SCE}) of immersion at 90ºC. Left: Nyquist diagrams. Right: Bode diagrams. Symbols: experimental results. .Lines: theoretical CNLS fitting using equivalent circuit of Figure 1.

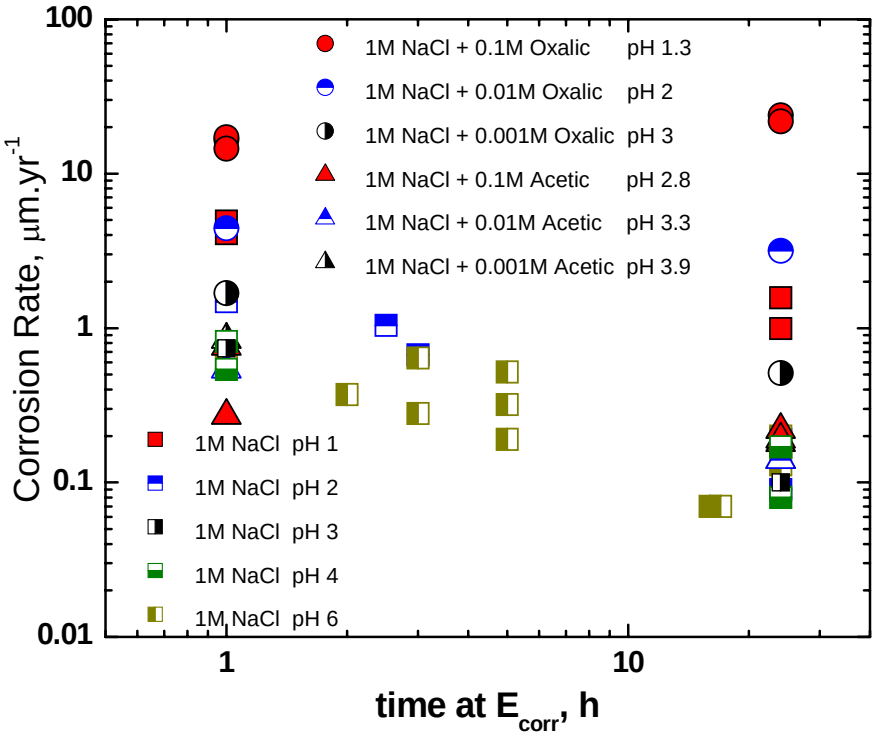

FIGURE 10: Variation of the Corrosion Rate at E_{corr} with time for Alloy 22 in naturally aerated 1M NaCl solutions with the addition of acetic or oxalic acid at 90ºC.

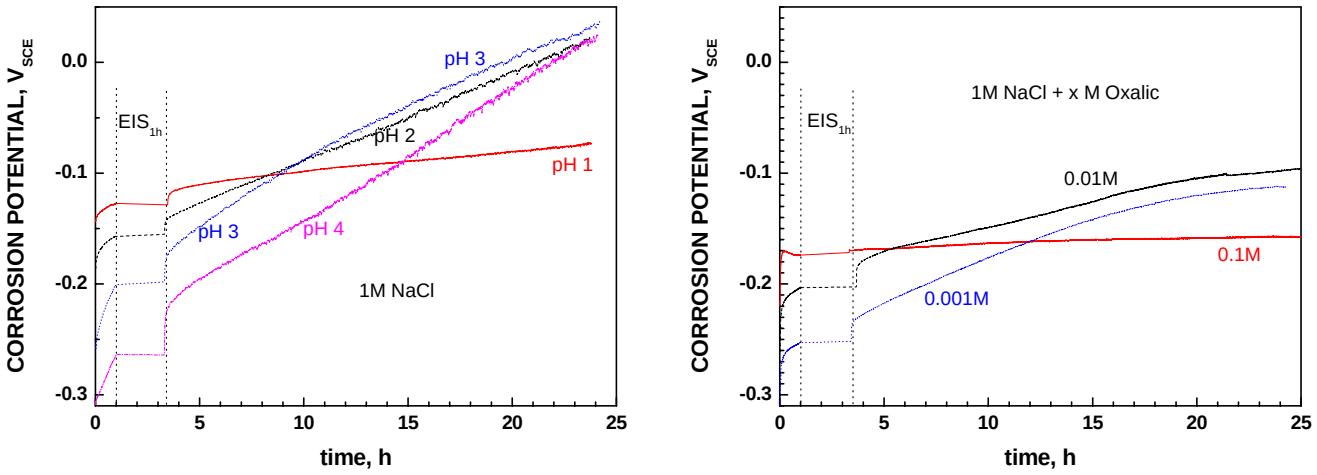

FIGURE 11: Variation of the Corrosion Potential with time for Alloy 22 in naturally aerated 1M NaCl solutions and in 1M NaCl with the addition of oxalic acid at 90ºC. The break of the curves at correspond to EIS measurements after 1h of immersion.

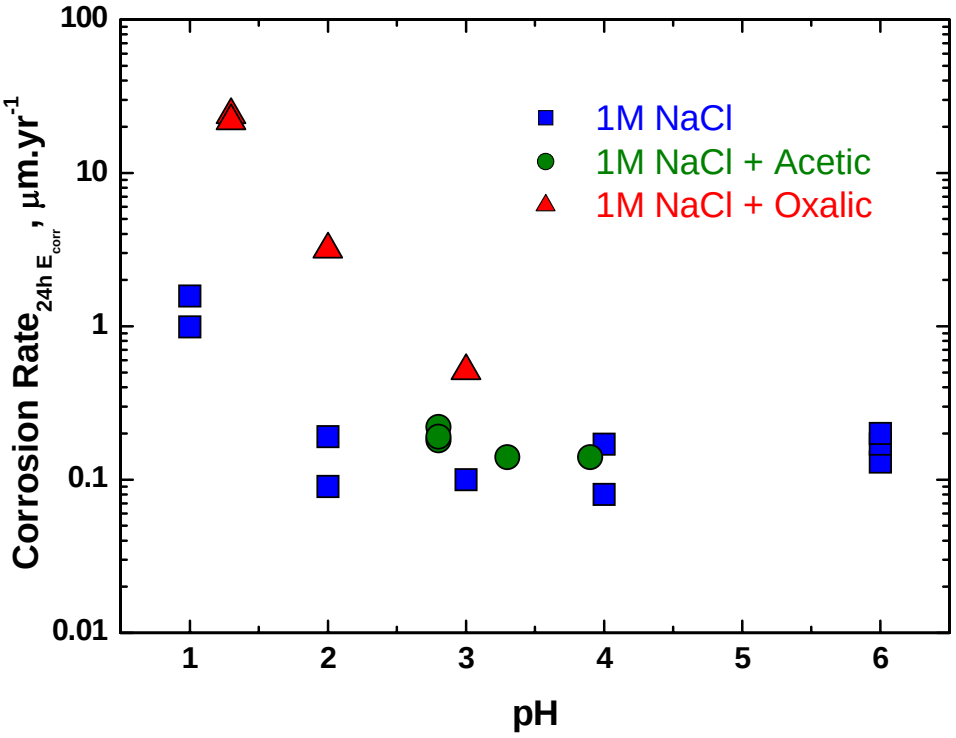

FIGURE 12: Variation of the Corrosion Rate measured after 24h at E_{corr} with solution pH for Alloy 22 in naturally aerated 1M NaCl solutions with the addition of acetic or oxalic acid at 90ºC.